Nanoscale

PAPER

View Article Online
View Journal | View Issue

Cite this: *Nanoscale*, 2025, **17**, 2235

Blister test to measure the out-of-plane shear modulus of few-layer graphene†

Metehan Calis, [a] Narasimha Boddeti[b] and J. Scott Bunch*[a,c]

Received 11th October 2024,
Accepted 4th December 2024

DOI: 10.1039/d4nr04214j

rsc.li/nanoscale

We measure the out-of-plane shear modulus of few-layer graphene (FLG) by a blister test. During the test, we employed a monolayer molybdenum disulfide (MoS_2) membrane stacked onto FLG wells to facilitate the separation of FLG from the silicon oxide (SiO_x) substrate. Using the deflection profile of the blister, we determine an average shear modulus G of 0.97 ± 0.15 GPa, and a free energy model incorporating the interfacial shear force is developed to calculate the adhesion energy between FLG and SiO_x substrate. The experimental protocol can be extended to other two-dimensional (2D) materials and layered structures (LS) made from other materials (WS_2, hBN, *etc.*) to characterize their interlayer interactions. These results provide valuable insight into the mechanics of 2D nano devices which is important in designing more complex flexible electronic devices and nanoelectromechanical systems.

1. Introduction

Atomically thin graphene, known for its high elastic modulus (Young's modulus ~1 TPa),[1] extreme bendability,[2] and conformity[3] to a surface, is a great candidate for flexible electronics[4] and soft robotics applications[5] as it can bend and shape into complex structures. Nevertheless, while research on 2D materials and their LS has predominantly concentrated on electrical and optical characterization, there has been a lack of focus on the characterization of the mechanical properties and interactions between the layers of these structures. Moreover, as the thickness reduces to the atomic level, surface forces play a critical role in device fabrication and functionality. For instance, the majority of fabrication processes entail transferring 2D materials from one substrate to another by utilizing van der Waals transfer methods.[6,7] Therefore, a comprehensive understanding of the mechanical properties of 2D materials, both in monolayer and layered configurations, is critical.

There is a growing body of literature demonstrating the strong adhesion energies between 2D materials and various substrates along with the high elastic moduli of these materials. However, one less studied but nevertheless important elastic constant is the shear modulus. The shear modulus which influences the bending rigidity and flexibility is of great importance to van der Waals bonded 2D materials and LSs. The shear modulus plays a role in how the structure folds,[8] ripples,[9] and slips.[10] Therefore, determining the shear modulus precisely has critical importance.[11] While much is understood about the shear modulus in bulk form of 2D materials such as graphite, less is known about the shear modulus in thin 2D materials and their LSs made from 2D materials. The majority of existing relevant research is based on computational modeling[12–15] and there is only a limited number of experimental studies[8,16–18] focused on the out-of-plane shear modulus of few-layer 2D systems.

2. Materials and methods

2.1. Materials and measurements

Here, we introduce a new approach to determining the out-of-plane shear modulus of an FLG by using a constant-N pressurized blister test which has been widely used to determine several mechanical properties of 2D thin-films including Young's modulus,[19] adhesion energies,[20,21] coefficient of friction,[22] and shear stress.[10] To fabricate the devices used in the blister test, we start with mechanical exfoliation of FLG over a SiO_x/Si wafer. Subsequently, we etch microcavities through the FLG, and SiO_x, and into the Si substrate (see the ESI for

[a]*Boston University, Department of Mechanical Engineering, Boston, MA 02215, USA*
[b]*Washington State University, School of Mechanical and Materials Engineering, Pullman, WA 99163, USA*
[c]*Boston University, Division of Materials Science and Engineering, Brookline, MA 02446, USA. E-mail: bunch@bu.edu*

† Electronic supplementary information (ESI) available: CVD growth and characterization, FLG well fabrication and MoS_2 layers transfer procedures, Young's modulus calculation, shear modulus derivation, and free energy model, investigation of the delamination behavior of the LS System by varying the thickness, Raman spectroscopy analysis over the delaminated blister, bending modulus and bending strain energy calculation, thickness dependence of delaminated LS profile, non-circular delamination examples. See DOI: https://doi.org/10.1039/d4nr04214j

details†). Then, we use an optical microscope[23] to identify FLG flakes on the substrates that fall within 10 to 50 layers of graphene thickness. Subsequently, we verify their thickness with the atomic force microscope (AFM).[24] Next, utilizing a micromanipulator, a chemical vapor deposition (CVD)-grown monolayer MoS_2 flake is transferred over the wells to cover the microcavities that are etched through the exfoliated FLG. This transferred MoS_2 flake enables us to lift and delaminate the FLG at the end of the blister test (Fig. 1a) (see the ESI†). After fabrication, the devices are placed into a pressure chamber and charged to a certain input pressure (p_0) with argon gas. The gas molecules diffuse into the sealed microcavity and we wait (~48 hours) until the input pressure and internal pressure (p_{int}) equilibrate ($p_0 = p_{int}$).[25] After taking the devices out of the pressure chamber, p_{int} is greater than p_{ext} ($p_{ext} \equiv p_{atm} \approx 1$ atm), and the MoS_2 membrane bulges upward which we image using the AFM. The devices are then returned to the pressure chamber at a higher p_0 and this process is repeated at this new input pressure (Fig. 1b left). Initially, the bulge radius is equal to the well radius (a_0) and the deflected MoS_2 behaves as a pressurized circular membrane clamped along the well boundary[25] by the adhesive forces between the MoS_2 membrane and the FLG. We use Hencky's model to determine the two-dimensional Young's modulus (E_{2D})[3,19,20,24,26] of MoS_2 (see the ESI for details†). Beyond a critical pressure, the pressure load on the MoS_2/FLG LS is large enough to overcome the adhesive forces clamping the MoS_2/FLG LS to the SiO_x surface, and it delaminates from the surface (Fig. 1b, right). In Fig. 1c, we show an AFM image of the device before (top) and after delamination (bottom). In Fig. 1d, we show cross-sections of the AFM scans of a device, which pass through the center of the blister, corresponding to varying input pressures. Some devices undergo multiple delaminations to larger radii (a) at higher pressures. We observe that the MoS_2/FLG LS delaminates from the substrate instead of just the MoS_2 membrane suggesting that the work of separation between MoS_2 and FLG

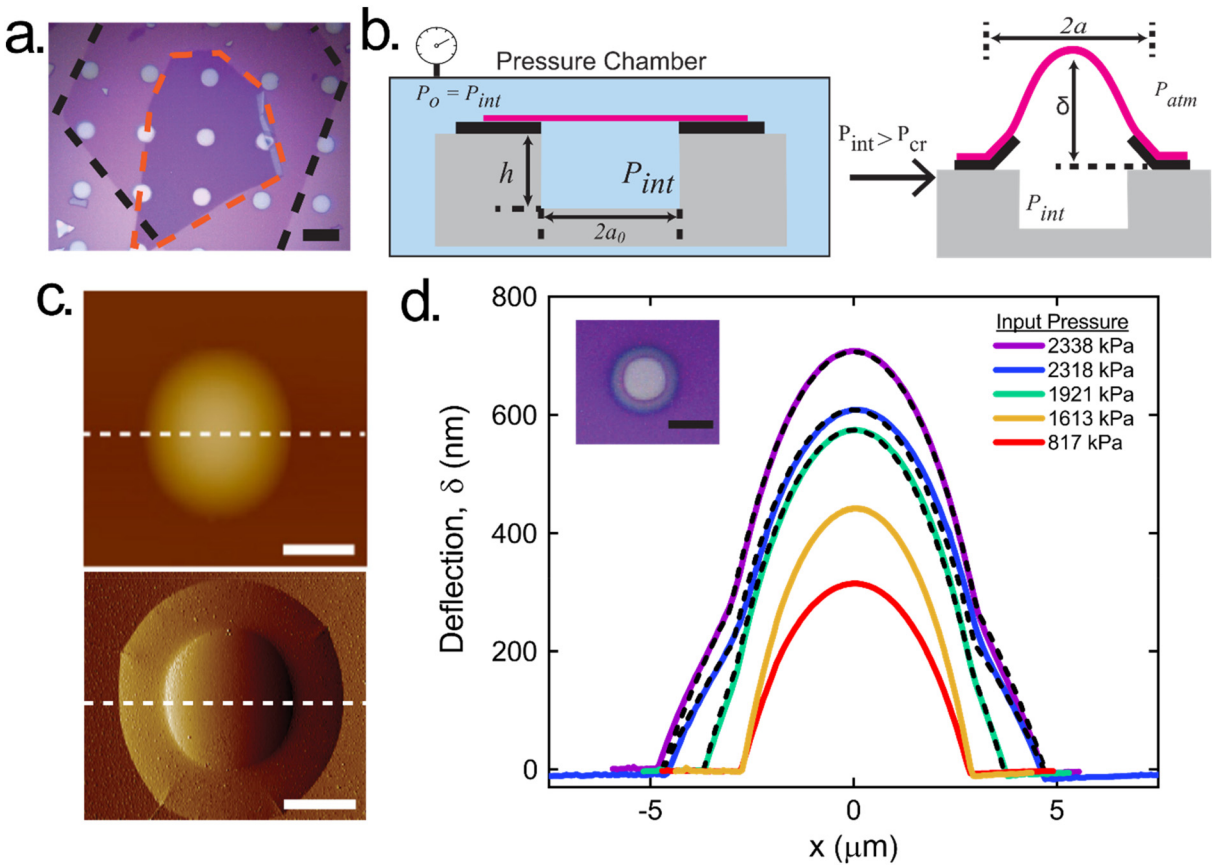

Fig. 1 (a) Optical image of the monolayer MoS_2 over the FLG substrate. The orange and black dashed lines show the boundary of monolayer MoS_2 flakes and FLG substrate, respectively. The scale bar is 10 μm. (b) Schematic illustration of the experimental procedure. Devices are kept in the pressure chamber until $p_0 = p_{int}$ (left). When the devices are taken out, the MoS_2 membrane bulges up due to $p_{int} > p_{ext}$ ($\approx p_{atm}$). This process is repeated with higher input pressures until the LS delamination is observed from the SiO_x surface ($p_{int} > p_{crt}$) (right) (pink: monolayer MoS_2 membrane, black: FLG, grey: SiO_x/Si substrate). (c) AFM height image of the MoS_2/FLG LS devices before (up) and AFM amplitude image after delamination (down). Scale bars are 2.5 μm. (d) Representative AFM cross-sections of the devices at various input pressures. In this particular device, we observed 3 LS delaminations. The dashed line curves are deflection profile fittings for the delaminated configurations, used to calculate the shear modulus. The kinks at the blisters become more pronounced as the input pressure increases. (Inset: optical image of the delaminated MoS_2/FLG LS device. Scale bar is 5 μm.)

is larger than that of FLG and SiO_x. In this delamination, unlike the typical blister configuration, we also observe a kink in the delamination profile where monolayer MoS_2 meets the FLG (Fig. 1d). This suggests that the FLG layer beneath the MoS_2 membrane has separated. We assume that all layers of the FLG delaminate with the MoS_2. However, there remains the possibility that some layers of FLG remain attached to the SiO_x surface.

fied Williams' model[31] for pressure-loaded clamped axisymmetric membranes by adding a shear term to the force balance equation. This allows us to determine the G_{2D} of the FLG when E_{2D} is known. In this model, we sub-divide the whole blister into two regions: (i) Region I ($r \le a_0$) where only MoS_2 is suspended, and (ii) Region II ($a_0 < r \le a$) comprised of the delaminated MoS_2/FLG LS. The deflection profiles, denoted as $w(r)$, of the delaminated LS device can be expressed as follows:

$$w(r) = \begin{cases} w_1(r) = \left(\dfrac{pa^4}{Et}\right)^{\frac{1}{3}} \sum\limits_{j=0,1,\ldots} C_j \zeta^{2j}, & \text{Region I } (r \le a_0) \\ w_2(r) = \left(\dfrac{pa^4}{Et}\right)^{\frac{1}{3}} \sum\limits_{j=0,1,\ldots} B_j (1 - \zeta^{(2j+2)}), & \text{Region II } (a_0 < r \le a) \end{cases} \quad (3)$$

2.2 Theoretical model

We model each MoS_2/FLG LS device as a thermodynamic system which includes the membrane, MoS_2/FLG LS-substrate interface, trapped gas, and external atmosphere. Our aim is to minimize the free energy of this system to determine its equilibrium configuration at any prescribed input pressure. We built our model based on previous studies,[3,27,28] and the free energy of the system can be expressed as:

$$F = F_{mem} + F_{gas} + F_{ext} + F_{adh} \quad (1)$$

F_{mem} is the strain energy of the membrane due to the pressure load assuming axisymmetric deformation, F_{gas} is the energy change due to the expansion of the gas molecules trapped in the blister, F_{ext} is the energy change of the external environment, and F_{adh} is the adhesion energy of the LS – substrate interface (see the ESI for further details†). We incorporate the following assumptions into our strain energy calculations: (1) stretching in the FLG layers is negligible[29] and the MoS_2/FLG LS experiences only shear deformation,[30] (2) the contribution of bending energy is neglected, and (3) a clamped boundary condition is valid.[19,25] We neglect the bending strain energy contribution to the free energy as it is negligible compared to the shear strain energy (see the ESI (Section 7) for more information†). Thus,

$$F_{mem} = \int_0^a \left(\frac{1}{2}(N_r\varepsilon_r + N_t\varepsilon_t)\right) 2\pi r \mathrm{d}r + \int_{a_0}^a \frac{1}{2} G_{2D} \left(\frac{\mathrm{d}w}{\mathrm{d}r}\right)^2 2\pi r \mathrm{d}r \quad (2)$$

where r is the radial coordinate, and w is transverse deflection. N_r and ε_r are the radial stress and strain, and N_t and ε_t are the circumferential stress and strain. G_{2D} is the two-dimensional shear modulus of FLG. We assume that the contribution of the MoS_2/FLG interface to G_{2D} is negligible, as the LS is largely composed of graphene layers. Therefore, G_{2D} can be calculated by multiplying the shear modulus (G) by the thickness of the layered structure ($G \times$ (thickness of LS) = G_{2D} (N/m)). We modified Williams' model[31] for pressure-loaded clamped axisymmetric membranes by adding a shear term to the force balance equation. This allows us to determine the G_{2D} of the FLG when E_{2D} is known. In this model, we sub-divide the whole blister into two regions: (i) Region I ($r \le a_0$) where only MoS_2 is suspended, and (ii) Region II ($a_0 < r \le a$) comprised of the delaminated MoS_2/FLG LS. The deflection profiles, denoted as $w(r)$, of the delaminated LS device can be expressed as follows:

where p is the pressure difference across the membrane ($p = p_{int} - p_{ext}$), t is the thickness of the membrane, and $\zeta = \frac{r}{a}$. The coefficients C_j and B_j are functions of $f_0 = 4G_{2D}/(E_{2D}p^2a^2)^{1/3}$ and are determined utilizing the governing equilibrium equations, clamped boundary conditions, and continuity of the displacements (see the ESI for further details†). We take E_{2D} of the MoS_2 layer ($E_{2D} = E_{bulk} \times$ (MoS_2 thickness)) as Young's modulus of the whole system since only the MoS_2 membrane is assumed to stretch by the pressure load. With f_0 as the fitting parameter, we fit the deflection profile from our model (dashed line in Fig. 1d) to the AFM cross-section of the delaminated blister configuration to determine f_0. Assuming isothermal expansion of a fixed number of gas molecules, the ideal gas law can be written as $p_0V_0 = p_{int}(V_0 + V_b)$ where V_0 is the initial volume of the microcavity. With the best-fit profile, we calculate the bulge volume (V_b) which allows us to determine the pressure difference p and thus, G_{2D}. Next, we incorporate the calculated G_{2D} value into the free energy model to find the adhesion energy between FLG and the SiO_x substrate when the blister reaches its equilibrium delaminated configuration.

3. Results and discussion

We measure the blister profile of each device that shows MoS_2/FLG LS delamination from the substrate, and in Fig. 2 we plot the shear modulus for 10 devices with nine of them delaminating multiple times (2 or 3 times). Additionally, any irregular and non-circular LS delaminations were not included in the analysis (see the ESI†). We find the average shear modulus for FLG to be $G = 0.97 \pm 0.15$ GPa. Our finding suggests that the primary contribution to the shear modulus of the LS is the FLG since the primary component of our experimental devices consists of graphite (FLG thickness range $\approx$ 4.25–6.25 nm *versus* monolayer MoS_2 thickness = 0.65 nm).[32] This value aligns with previous experimental studies on the out-of-plane shear modulus of various types of graphite (0.36–4.52 GPa) and is close to the value of $G = 4$ GPa for intrinsic dislocation-free graphite.[8,16–18]

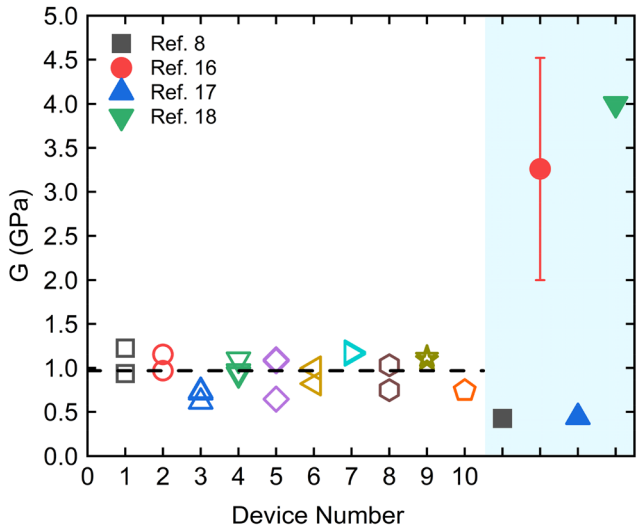

Fig. 2 Shear modulus of the 10 devices. 9 devices undergo multiple delaminations from the surface. The dashed line is the average of all devices (G = 0.97 ± 0.15 GPa). The data in the blue shaded box are taken from the literature.

The only unknown parameter remaining in the description of the thermodynamic system is the separation energy (Γ_{sep}) of the FLG layers from the SiO_x surface. Through an iterative process, we numerically determine the separation energy for each delaminated device by matching the theoretical system minimum with respect to a and p with the experimental observation. In Fig. 3a, we plot the free energy change of one device as a function of a and p. The red dot on the plot shows the free energy minimum that matches the experimental observation and thus provides us the separation energy. The separation energies thus obtained are shown in Fig. 3b, with the average Γ_{sep} = 0.20 ± 0.02 J m^{-2} shown as a dashed line. Our measured value for the separation energy aligns with previous studies[19,21,33] on the separation of multilayer graphene over SiO_x substrates. Our model can be extended to predict the delamination behavior of other LS devices that are made of other 2D materials (see the ESI†).

To explore the impact of the thickness of the FLG on the delamination behavior, we transfer monolayer MoS_2 onto FLG flakes with varying thicknesses, targeting a total LS thickness range of 2 nm to 11 nm since after a certain thickness of FLG, only MoS_2 membrane delaminates from the surface.[25] In Fig. 4, we show the optical microscope image along with thickness measurements and blister cross-sections. We include an example of a thinner device (2 nm) as shown in Fig. 4a where the kink on the blister profile of the LS delamination is not noticeable in the AFM scan (see the ESI for further details†). As the underlying graphite thickness in the LS approaches the thickness of the monolayer MoS_2 membrane, it is not possible to determine whether LS delamination has occurred or not since the layers of the delaminated LS blisters become more flexible and compatible with each other (see Fig. S8†). Consequently, we are unable to precisely fit the curve to the cross-section of the delaminated device, which makes the determination of G_{2D} for such devices difficult. Fig. 4b is an explanatory example in which we observe both only MoS_2 and MoS_2/FLG LS delaminations in two different devices at the same input pressure on the same multilayer graphene flake which is 6.3 nm thick. The thickness of all the devices utilized for the calculation of G_{2D} lay within the range of 5–7 nm. In contrast, as shown in Fig. 4c, above a certain graphite thickness, we observe only delamination of the MoS_2 membrane from the FLG surface. Additionally, as shown in Fig. 1c, thin MoS_2/FLG devices are prone to developing wrinkles which can affect the assumption of a fully clamped, axisymmetric profile. We neglect the effect of wrinkles because there is no simple analytical model available to accurately describe their influence.

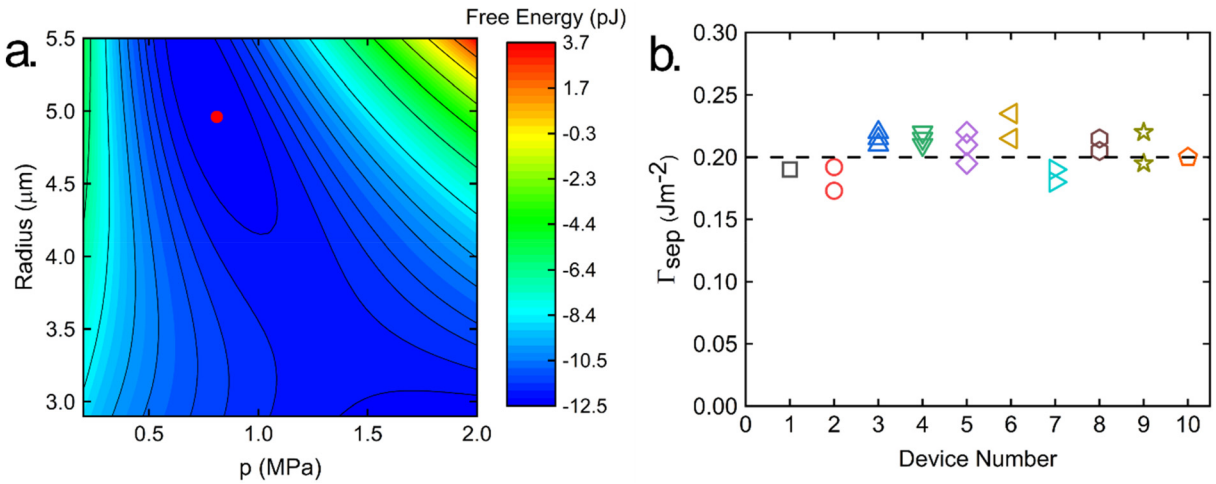

Fig. 3 (a) Filled contour plot of free energy change of MoS_2/FLG LS. The red dot in the plot shows the location of the minimum energy after delamination. (b) Separation energies of the MoS_2/FLG LS devices from SiO_x. Several devices were subjected to multiple delamination. The dashed line is the average of all devices (Γ_{sep} = 0.2 ± 0.02 J m^{-2}).

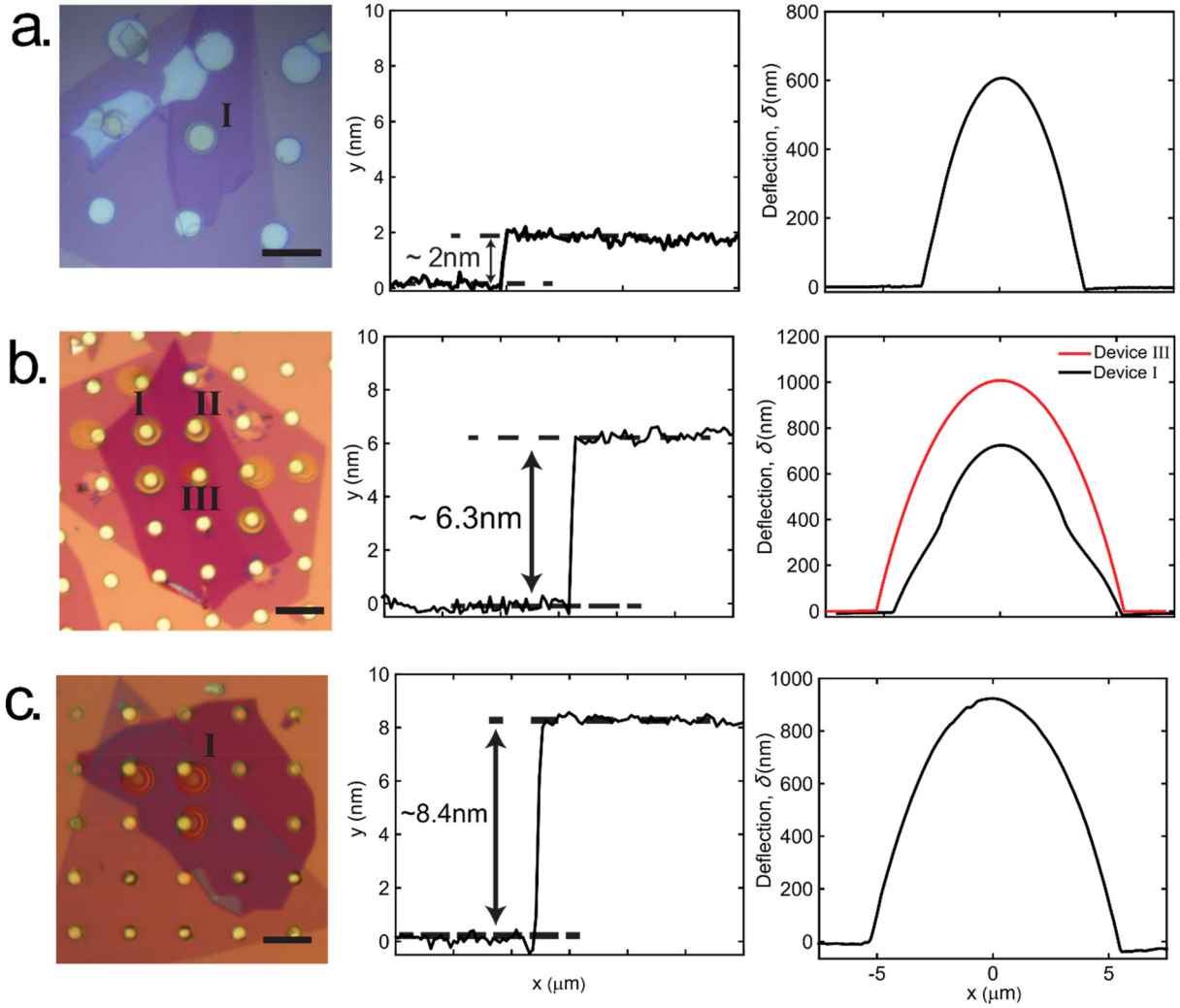

Fig. 4 (a) Optical image (left) of the 2 nm-thick device that shows LS delamination. The thickness of the LS (middle) and AFM cross-section (right) of the device (I). LS delamination is hard to observe with the AFM scan. The scale bar is 10 μm. (b) Optical image (left) of one of the LS devices. Blister-I is typical LS delamination from SiO_x, Blister-II is an LS delamination from SiO_x, and Blister-III is the regular delamination of MoS_2 from the FLG surface. The thickness of the LS (middle) and cross-section of the Blister-I and III (right). The scale bar is 20 μm. (c) Optical image (left) of MoS_2 on slightly thicker multilayer graphene. After a certain thickness, we only observe regular delamination of MoS_2 from the FLG surface. The thickness of the LS (middle) and cross-section of the Blister-I (right). The scale bar is 20 μm.

To further understand why we do not observe LS delamination for thicknesses exceeding a value of ~7 nm, we will compare the free energy variation at three different input pressures. In Fig. 5, we plot the variation in free energy according to: (i) the standard free energy model based on Hencky's solution that describes the delamination of the MoS_2 membrane from FLG (solid lines), and (ii) the LS free energy model that we utilize to describe the delamination of the MoS_2/FLG LS (dashed lines), both expressed as a function of the blister radius. In this demonstration, we focus on three different thicknesses of LS, 2 nm, 6 nm, and 9 nm. For each case, we use microcavity dimensions that represent the devices used in the experiment: depth of 600 nm and a radius of 2.5 μm and use the experimentally measured parameters $G = 0.97 \pm 0.15$ GPa, $\Gamma_{sep} = 0.20$ J m^{-2} (work of separation of graphite from SiO_x), $E_{2D} = 171.1$ N/m, and $\Gamma_{sep} = 0.39$ J m^{-2} (work of separation of MoS_2 from graphite) from our previous work.[25] For each free energy model, we locate the equilibrium configuration by finding the local minimum of the free energy functions (F) by setting its derivatives with respect to the independent variable a to zero ($dF/da = 0$). When the input pressure p_0 is below a critical pressure (p_{cr}) for delamination specific to the free energy model, the membrane stays pinned at the initial radius since there are no local minima above the well radius. When $p_0 = p_{cr}$, the system possesses an equilibrium configuration at $a = a_0$ and further input pressure increase beyond this point results in delamination to $a > a_0$, and F reaches its local minimum (the part of the curve with $a < a_0$ is not observable physically).

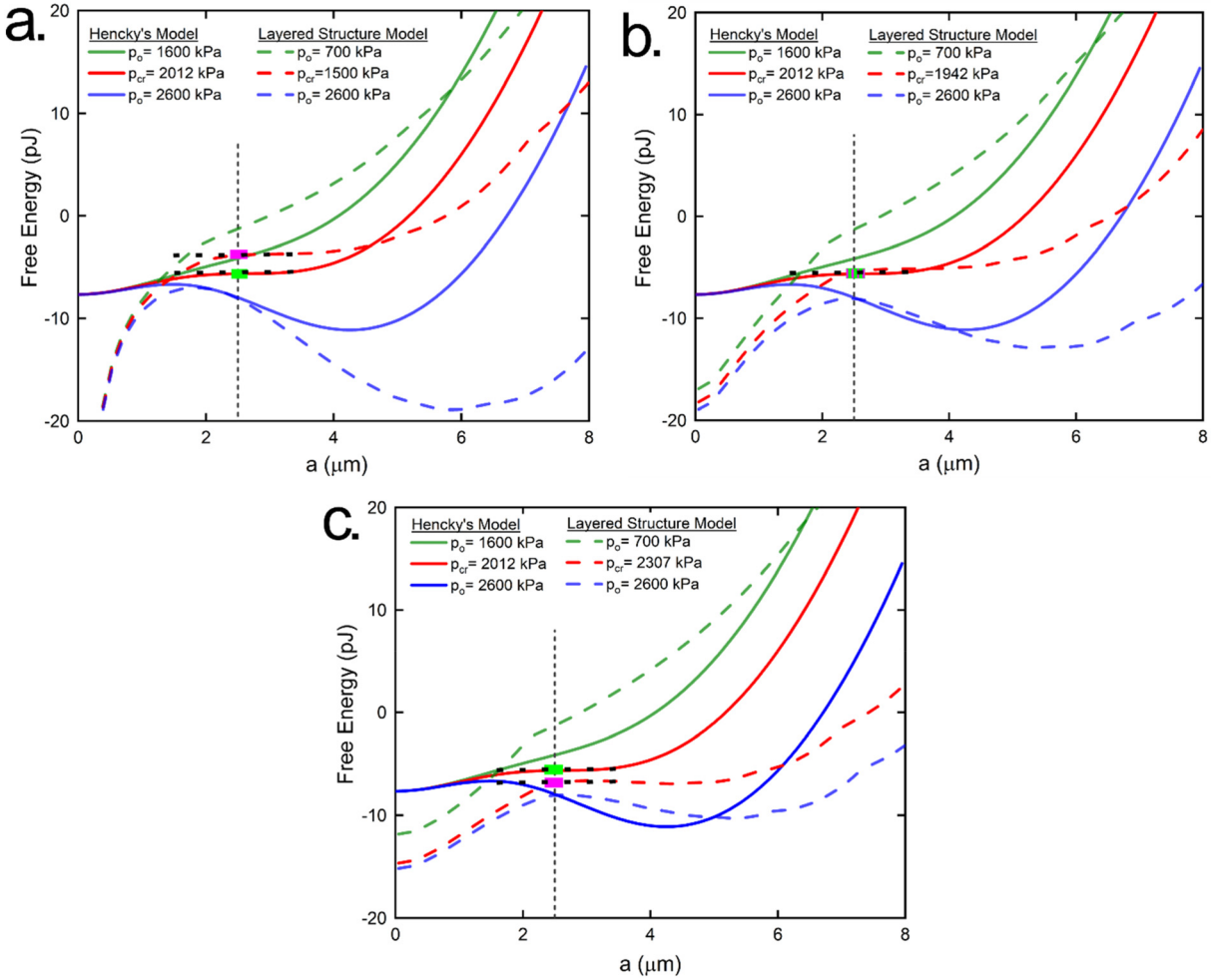

Fig. 5 Comparison of free energy models at 3 different p_o. The black vertical dashed line shows the well radius. Rectangular symbols indicate the equilibrium configuration where $dF/da = 0$. MoS_2/FLG thickness (a) 2 nm, (b) 6 nm, and (c) 9 nm.

In Fig. 5a (LS thickness: 2 nm), we can see that the LS model possesses a local minimum at the edge of the well at an input pressure lower than the standard blister model. Therefore beyond this critical pressure p_{cr}, for the LS model, the system will follow the minimum of the LS model and LS delamination is expected. In Fig. 5b (LS thickness: 6 nm), the local minima for both free energy models occur around the same critical input pressure. Thus variation in the adhesion strength or the local van der Waals interactions play a crucial role in determining whether the system follows one path or the other for the delamination configuration (see the ESI for details on identifying the delamination transition zone†). As FLG thickness increases, MoS_2 membrane separation from the FLG surface becomes thermodynamically more favorable than FLG delamination from the SiO_x substrate and FLG shearing. In Fig. 5c, with thicker FLG layer combinations (LS thickness: 9 nm), the standard model reaches a local minimum before the LS model. So only MoS_2 separates from the graphite surface and no LS delamination takes place.

4. Conclusion

We conducted a study on the mechanical behavior of a FLG using the constant-N blister test. By increasing the input pressure, causing the MoS_2 membrane to bulge upwards, we successfully induced delamination of the MoS_2/FLG LS from the SiO_x surface. Analyzing the blister configuration as a thermodynamic system, we measure the shear modulus of the FLG as $G = 0.97 \pm 0.15$ GPa and $\Gamma_{sep} = 0.20 \pm 0.02$ J m^{-2} for separation energy for FLG from SiO_x surface. We also calculated the critical pressure and thickness relation to demonstrate that beyond ~7 nm thickness of MoS_2/FLG, we do not observe LS delamination. Our study is useful for understanding the mechanical behavior of layered 2D structures and can be extended to determine the shear modulus of 2D layered heterostructures. This can be used to guide the development of new designs of electrical and mechanical systems in flexible electronic[34] and soft robotics applications[35] or the fabrication of more complex structures based on 2D heterostructure materials.[36,37]

Author contributions

Metehan Calis: formal analysis, data curation, writing – review & editing, writing – original draft. J. Scott Bunch: writing – review & editing, supervision, conceptualization. Narasimha Boddeti: writing – review & editing, supervision, conceptualization, formal analysis.

Data availability

The data supporting this article have been included as part of the ESI. Any additional and raw data that were used during the preparation of the manuscript and ESI are available from the corresponding author upon request.†

Conflicts of interest

There are no conflicts to declare.

Acknowledgements

This work was funded by the Ministry of National Education of Turkey under the Graduate Education Scholarship (YLSY) program.

References

1 C. Lee, X. Wei, J. W. Kysar and J. Hone, Measurement of the Elastic Properties and Intrinsic Strength of Monolayer Graphene, *Science*, 2008, **321**(5887), 385–388, DOI: **10.1126/science.1157996**.

2 Y. Wei and R. Yang, Nanomechanics of Graphene, *Natl. Sci. Rev.*, 2019, **6**(2), 324–348, DOI: **10.1093/NSR/NWY067**.

3 N. G. Boddeti, R. Long and M. L. Dunn, Adhesion Mechanics of Graphene on Textured Substrates, *Int. J. Solids Struct.*, 2016, **97–98**, 56–74, DOI: **10.1016/J.IJSOLSTR.2016.07.043**.

4 H. Jang, Y. J. Park, X. Chen, T. Das, M. S. Kim and J. H. Ahn, Graphene-Based Flexible and Stretchable Electronics, *Adv. Mater.*, 2016, **28**(22), 4184–4202, DOI: **10.1002/ADMA.201504245**.

5 S. Wang, Y. Gao, A. Wei, P. Xiao, Y. Liang, W. Lu, C. Chen, C. Zhang, G. Yang, H. Yao and T. Chen, Asymmetric Elastoplasticity of Stacked Graphene Assembly Actualizes Programmable Untethered Soft Robotics, *Nat. Commun.*, 2020, **11**(1), 1–12, DOI: **10.1038/s41467-020-18214-0**.

6 Z. Huang, A. Alharbi, W. Mayer, E. Cuniberto, T. Taniguchi, K. Watanabe, J. Shabani and D. Shahrjerdi, Versatile Construction of van Der Waals Heterostructures Using a Dual-Function Polymeric Film, *Nat. Commun.*, 2020, **11**(1), 1–10, DOI: **10.1038/s41467-020-16817-1**.

7 F. Liu, W. Wu, Y. Bai, S. H. Chae, Q. Li, J. Wang, J. Hone and X. Y. Zhu, Disassembling 2D van Der Waals Crystals into Macroscopic Monolayers and Reassembling into Artificial Lattices, *Science*, 2020, **367**(6480), 903–906, DOI: **10.1126/SCIENCE.ABA1416**.

8 X. Chen, C. Yi and C. Ke, Bending Stiffness and Interlayer Shear Modulus of Few-Layer Graphene, *Appl. Phys. Lett.*, 2015, **106**(10), 101907, DOI: **10.1063/1.4915075**.

9 N. Haghighian, D. Convertino, V. Miseikis, F. Bisio, A. Morgante, C. Coletti, M. Canepa and O. Cavalleri, Rippling of Graphitic Surfaces: A Comparison between Few-Layer Graphene and HOPG, *Phys. Chem. Chem. Phys.*, 2018, **20**(19), 13322–13330, DOI: **10.1039/C8CP01039K**.

10 G. Wang, Z. Dai, Y. Wang, P. Tan, L. Liu, Z. Xu, Y. Wei, R. Huang and Z. Zhang, Measuring Interlayer Shear Stress in Bilayer Graphene, *Phys. Rev. Lett.*, 2017, **119**(3), 036101, DOI: **10.1103/PHYSREVLETT.119.036101**.

11 X. Liu, T. H. Metcalf, J. T. Robinson, B. H. Houston and F. Scarpa, Shear Modulus of Monolayer Graphene Prepared by Chemical Vapor Deposition, *Nano Lett.*, 2012, **12**(2), 1013–1017, DOI: **10.1021/NL204196V**.

12 T. Mukhopadhyay, A. Mahata, S. Adhikari and M. Asle Zaeem, Probing the Shear Modulus of Two-Dimensional Multiplanar Nanostructures and Heterostructures, *Nanoscale*, 2018, **10**(11), 5280–5294, DOI: **10.1039/C7NR07261A**.

13 B. Hajgató, S. Güryel, Y. Dauphin, J. M. Blairon, H. E. Miltner, G. Van Lier, F. De Proft and P. Geerlings, Out-of-Plane Shear and out-of Plane Young's Modulus of Double-Layer Graphene, *Chem. Phys. Lett.*, 2013, **564**, 37–40, DOI: **10.1016/J.CPLETT.2013.02.018**.

14 K. Min and N. R. Aluru, Mechanical Properties of Graphene under Shear Deformation, *Appl. Phys. Lett.*, 2011, **98**(1), 013113, DOI: **10.1063/1.3534787**.

15 G. Savini, Y. J. Dappe, S. Öberg, J. C. Charlier, M. I. Katsnelson and A. Fasolino, Bending Modes, Elastic Constants and Mechanical Stability of Graphitic Systems, *Carbon*, 2011, **49**(1), 62–69, DOI: **10.1016/J.CARBON.2010.08.042**.

16 O. L. Blakslee, D. G. Proctor, E. J. Seldin, G. B. Spence and T. Weng, Elastic Constants of Compression–Annealed Pyrolytic Graphite, *J. Appl. Phys.*, 1970, **41**(8), 3373–3382, DOI: **10.1063/1.1659428**.

17 M. Rejhon, F. Lavini, A. Khosravi, M. Shestopalov, J. Kunc, E. Tosatti and E. Riedo, Relation between Interfacial Shear and Friction Force in 2D Materials, *Nat. Nanotechnol.*, 2022, **17**(12), 1280–1287, DOI: **10.1038/s41565-022-01237-7**.

18 E. J. Seldin and C. W. Nezbeda, Elastic Constants and Electron–Microscope Observations of Neutron–Irradiated Compression–Annealed Pyrolytic and Single–Crystal Graphite, *J. Appl. Phys.*, 1970, **41**(8), 3389–3400, DOI: **10.1063/1.1659430**.

19 N. G. Boddeti, S. P. Koenig, R. Long, J. Xiao, J. S. Bunch and M. L. Dunn, Mechanics of Adhered, Pressurized Graphene Blisters, *ASME. J. Appl. Mech.*, 2013, **80**(4), DOI: **10.1115/1.4024255**.

20 D. Lloyd, X. Liu, N. Boddeti, L. Cantley, R. Long, M. L. Dunn and J. S. Bunch, Adhesion, Stiffness, and Instability in Atomically Thin MoS2 Bubbles, *Nano Lett.*, 2017, **17**(9), 5329–5334, DOI: **10.1021/acs.nanolett.7b01735**.

21 S. P. Koenig, N. G. Boddeti, M. L. Dunn and J. S. Bunch, Ultrastrong Adhesion of Graphene Membranes, *Nat. Nanotechnol.*, 2011, **6**(9), 543–546, DOI: **10.1038/nnano.2011.123**.

22 A. L. Kitt, Z. Qi, S. Rémi, H. S. Park, A. K. Swan and B. B. Goldberg, How Graphene Slides: Measurement and Theory of Strain-Dependent Frictional Forces between Graphene and SiO_2, *Nano Lett.*, 2013, **13**(6), 2605–2610, DOI: **10.1021/NL4007112**.

23 H. Li, J. Wu, X. Huang, G. Lu, J. Yang, X. Lu, Q. Xiong and H. Zhang, Rapid and Reliable Thickness Identification of Two-Dimensional Nanosheets Using Optical Microscopy, *ACS Nano*, 2013, **7**(11), 10344–10353, DOI: **10.1021/NN4047474**.

24 H. Hencky, Ueber Den Spannungszustand in Kreisrunden Platten Mit Verschwindender Biegungssteifigkeit, *Z. Math. Phys.*, 1915, **63**, 311–317.

25 M. Calis, D. Lloyd, N. Boddeti and J. S. Bunch, Adhesion of 2D MoS2 to Graphite and Metal Substrates Measured by a Blister Test, *Nano Lett.*, 2023, **23**(7), 2607–2614, DOI: **10.1021/ACS.NANOLETT.2C04886**.

26 W. B. Fichter, Some Solutions for the Large Deflections of Uniformly Loaded Circular Membranes, *NASA Tech. Pap.*, 1997, **3658**, 1–24.

27 Y. Ma, G. Wang, Y. Chen, D. Long, Y. Guan, L. Liu and Z. Zhang, Extended Hencky Solution for the Blister Test of Nanomembrane, *Extreme Mech. Lett.*, 2018, **22**, 69–78, DOI: **10.1016/J.EML.2018.05.006**.

28 Z. C. Huang, Z. Z. He, Y. B. Zhu and H. A. Wu, A General Theory for the Bending of Multilayer van Der Waals Materials, *J. Mech. Phys. Solids*, 2023, **171**, 105144, DOI: **10.1016/J.JMPS.2022.105144**.

29 K.-T. Wan and S.-C. Lim, The Bending to Stretching Transition of a Pressurized Blister Test, *Int. J. Fract.*, 1998, **92**(4), 43–47, DOI: **10.1023/A:1007612016147**.

30 E. Han, J. Yu, E. Annevelink, J. Son, D. A. Kang, K. Watanabe, T. Taniguchi, E. Ertekin, P. Y. Huang and A. M. van der Zande, Ultrasoft Slip-Mediated Bending in Few-Layer Graphene, *Nat. Mater.*, 2019, **19**(3), 305–309, DOI: **10.1038/s41563-019-0529-7**.

31 J. G. Williams, Energy Release Rates for the Peeling of Flexible Membranes and the Analysis of Blister Tests, *Int. J. Fract.*, 1997, **87**(3), 265–288, DOI: **10.1023/A:1007314720152**.

32 X. Li and H. Zhu, Two-Dimensional MoS2: Properties, Preparation, and Applications, *J. Mater.*, 2015, **1**(1), 33–44, DOI: **10.1016/J.JMAT.2015.03.003**.

33 H. Rokni and W. Lu, Direct Measurements of Interfacial Adhesion in 2D Materials and van Der Waals Heterostructures in Ambient Air, *Nat. Commun.*, 2020, **11**(1), 1–14, DOI: **10.1038/s41467-020-19411-7**.

34 D. De Fazio, I. Goykhman, D. Yoon, M. Bruna, A. Eiden, S. Milana, U. Sassi, M. Barbone, D. Dumcenco, K. Marinov, A. Kis and A. C. Ferrari, High Responsivity, Large-Area Graphene/MoS2 Flexible Photodetectors, *ACS Nano*, 2016, **10**(9), 8252–8262, DOI: **10.1021/ACSNANO.6B05109**.

35 L. Jing, K. Li, H. Yang and P. Y. Chen, Recent Advances in Integration of 2D Materials with Soft Matter for Multifunctional Robotic Materials, *Mater. Horiz.*, 2020, **7**(1), 54–70, DOI: **10.1039/C9MH01139K**.

36 W. Lee, Y. Liu, Y. Lee, B. K. Sharma, S. M. Shinde, S. D. Kim, K. Nan, Z. Yan, M. Han, Y. Huang, Y. Zhang, J. H. Ahn and J. A. Rogers, Two-Dimensional Materials in Functional Three-Dimensional Architectures with Applications in Photodetection and Imaging, *Nat. Commun.*, 2018, **9**(1), 1–9, DOI: **10.1038/s41467-018-03870-0**.

37 Z. Zhang, Z. Tian, Y. Mei and Z. Di, Shaping and Structuring 2D Materials via Kirigami and Origami, *Mater. Sci. Eng., R*, 2021, **145**, 100621, DOI: **10.1016/J.MSER.2021.100621**.